*Journal of*
*Nanoscience and Nanotechnology*
Vol. 11, 1–6, 2011

# Cathodoluminescence Evaluation of Defect Structure in Hydrothermally Grown ZnO:Sb Nanorods

A. González[1, 2], M. Herrera[2, *], J. Valenzuela[2], A. Escobedo[3, 4], and U. Pal[3]

[1] *Posgrado en Física de Materiales, Centro de Investigación Científica y de Educación Superior de Ensenada, Apartado Postal 2732, Ensenada, B. C. 22860, México.*
[2] *Centro de Nanociencias y Nanotecnología, Universidad Nacional Autónoma de México, Apdo. Postal 356, Ensenada, B.C. 22800, México*
[3] *Instituto de Física, Benemérita Universidad Autónoma de Puebla, Apdo. Postal J-48, Puebla, Pue. 72570, México*
[4] *Facultad de Ingeniería Química, Benemérita Universidad Autónoma de Puebla, Apdo. Postal J-48, Puebla, Pue. 72570, México*

Cathodoluminescence emission of hydrothermally grown antimony doped ZnO nanostructures with different antimony doping (2.5, 4.8, and 11.8 at%) was studied in a scanning electron microscope (CL-SEM). Incorporation of antimony results in formation of mostly nanorods with low aspect ratio together with some Sb-rich nanoparticles. Transmission electron microscopy (TEM) of the Sb-doped samples revealed delaminated {10–10} planes produced by antimony surface segregation. CL spectra of the as-grown samples revealed well defined emission bands centered at 3.2, 2.74 and 2.0 eV, attributed to excitonic recombination, and the so-called blue and yellow emissions, respectively. It was observed that the intensity of the blue emission depends strongly on antimony content, suggesting the formation of point defects on Sb doping. While the yellow emission red-shifted after thermal annealing, either in argon or oxygen atmosphere, the intensity of the blue band decreases considerably; such behavior is explained through the reduction of the population of $Zn_i$ defects.

**Keywords:** ZnO, Nanorods, Antimony Doping, Cathodoluminescence.

RESEARCH ARTICLE

## 1. INTRODUCTION

Zinc oxide (ZnO), a direct and wide band gap semiconductor (3.3 eV at 300 K) is currently one of the most studied materials due to its excellent electrical, optical and optoelectronic properties, promising to be a good candidate for the fabrication of optoelectronic devices, such as highly efficient blue lasers and UV, blue and white light-emitting diodes,[1] field-effect transistors,[2] gas sensors,[3] photovoltaic cells,[4] etc. All of these potential applications for ZnO are due to its wide band gap and large exciton binding energy (60 meV), larger than other semiconductor materials such as ZnSe (22 meV) and GaN (25 meV). For device applications, it is necessary to induce both *n*-and *p*-type conductivity in ZnO. Incorporation of doping atoms like Al, In, Sn and Ga has been tried in order to induce *n*-type conductivity,[5–9] and N and P for *p*-type conductivity.[10–12] Very recently, Sb was used to produce *p*-type ZnO thin films and nanostructures. Their optoelectronic properties were studied using different luminescent techniques like photoluminescence (PL), electroluminescence (EL), and cathodoluminescence.[13–16] However, incorporation of impurities in semiconductors frequently produces crystalline defects that generate undesired luminescence or diminish some emissions due to generation of non-radiative centers, sometimes induced by heavy doping.[14]

Cathodoluminescence (CL), besides photoluminescence, is a widely used technique for defect characterization in semiconductors due to its high sensibility and spatial resolution to detect significant changes in optical properties induced by impurities/doping, even at low concentrations, like the spectral and spatial distribution of defect related emissions in ZnO nanostructures.[17] Perhaps the most well-known defect related emission in ZnO is the broad yellow emission centered at about of 2.2 eV, where the peak position and intensity depend strongly on the growth method.[18] This visible emission has been frequently related to the presence of native point defects,[19] extrinsic, and complex defects.[20] Previously we reported two component bands centred at about 1.77 eV y 2.24 eV for this broad visible emission in ZnO nanostructures.[21]

In this article, we present a detailed CL study on the generation of point defects in ZnO nanorods through

*Author to whom correspondence should be addressed.

incorporation of antimony. The effects of Sb doping and thermal annealing on the morphology and defect structures of ZnO nanostructures are discussed.

## 2. EXPERIMENTAL DETAILS

Undoped and Sb doped ZnO nanostructures were grown through a low-temperature hydrothermal process, following the procedure reported earlier.[22] Zinc acetate dihydrate [$Zn(CH_3COO)_2 \cdot 2H_2O$; Aldrich, 99.99%], antimony acetate [$Sb(CH_3COO)_2$; Aldrich, 99.99%], ethylenediamine [$NH_2(CH_2)_2NH_2$; J.T. Baker, 99.9%], and sodium hydroxide [NaOH; Aldrich, 99.99%] were used without further purification. In a typical synthesis process, in a round bottom flask an alkaline solution of deionized water and ethylenediamine (9:1 v/v) was prepared. Afterwards 10.25 g of zinc acetate dihydrate was dissolved under vigorous stirring, and a measured amount of NaOH was incorporated into the solution until a pH of 12 was reached. The prepared solution was hydrothermally treated at 110 °C for 15 h and subsequently cooled freely to room temperature. The final products were extracted by decantation and washed several times with deionized water and dried in a muffle furnace (>100 °C). For Sb doping, different amounts of antimony acetate was added to the aqueous solution in order to obtain the desired nominal doping of 0.5, 1.0 and 2.0 at%. All the obtained samples were annealed at 500 °C for 1 h under oxygen or argon flow.

For SEM and EDS analysis, powder samples were placed over graphite tape or silver paint adhered to a copper sample-holder. The samples were analyzed in a JEOL JSM 5300 SEM microscope, using electron beam energy of 15 keV. Along with EDS analysis, inductively coupled plasma (ICP) measurements were performed to determine the Sb content in doped samples (Table I). For ICP measurements, powder samples were digested in 3 ml of concentrated HCl and filled up to 50 ml with deionized water. A Thermo Electron ICAP 6500 ICP-OES system was used for this purpose. A JEOL JEM-2010 transmission electron microscope (TEM) operating at 200 keV was used to study changes in nanorod morphology due to thermal annealing. CL measurements were performed at room and low temperature (100 K) in the UV-visible spectral range. CL signal was generated by using the electron beam of a scanning electron microscope as excitation source. A Hamamatsu R928P photomultiplier tube and a SPEX 340E monochromator were used for spectral analysis.

**Table I.** Sb content in ZnO:Sb nanostructures measured through EDS and ICP analysis.

| | Sb concentration (Atomic%) | | |
|---|---|---|---|
| Sample | Nominal | EDS | ICP |
| 1 | — | 0.00 | 0.00 |
| 2 | 0.5 | 0.19 | 2.56 |
| 3 | 1.0 | 0.50 | 4.88 |
| 4 | 2.0 | 1.67 | 11.85 |

## 3. RESULTS AND DISCUSSION

Secondary electron images from sample 1 show the formation of tapered needle shaped ZnO nanostructures with diameter in between 100 and 650 nm, and 4 $\mu$m average length [Fig. 1(a)]. From Figure 1 it can be seen that the morphology of the nanostructures changed drastically with increased Sb doping, from prismatic nanorods with increasingly shorter lengths in samples 2 and 3 [Figs. 1(b) and (c) respectively], to clustered particles in sample 4 [Fig. 1(d)]. Sample 2 and 3 also reveal a fairly uniform diameter distribution of 450 and 200 nm respectively, with several larger size structures in sample 3. Several nanoparticles could also be found in the sample 3 as shown in Figure 4 (arrows).

TEM images of the Sb doped samples revealed nanorods with an irregular surface in their lateral {10–10} planes, forming concentric ZnO layers at the ends (Fig. 2), suggesting a predominantly spiral growth of the crystal in the *c* direction. This phenomenon was observed only in Sb doped samples, and could be attributed to surface segregation of Sb. Previously, Kai et al. reported Sb segregation in ZnO grain boundaries, which induced the formation of bi-crystalline nanostructures.[23] Similarly, indium segregation in steps of a ZnO crystal was attributed be the cause of single crystal nanobelt growth.[24] Clearly the presence of the doping element affects the growth kinetics of ZnO crystals to form unusual structures.

Panchromatic CL images of undoped ZnO nanostructures reveal a homogeneous intensity distribution [Fig. 3(b)], with several nanorods that produce a more intense CL emission due to their higher thickness.

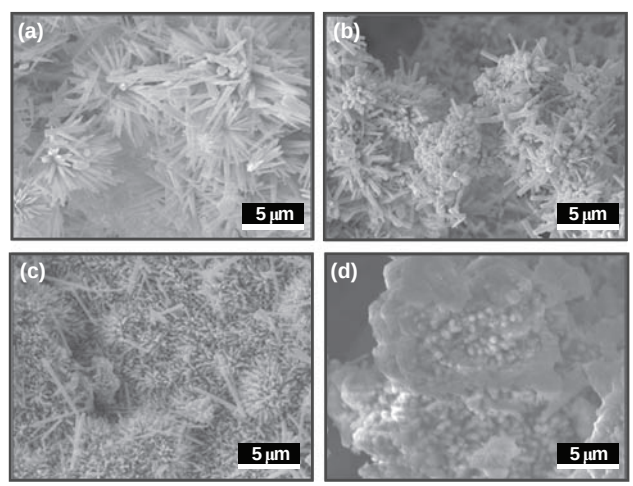


**Fig. 1.** Typical SEM images of undoped and antimony doped ZnO nanostructures. (a) Sample 1, (b) Sample 2 (2.5 %-Sb), (c) Sample 3 (4.8 %-Sb) and d) Sample 4 (11.8 %-Sb).



RESEARCH ARTICLE

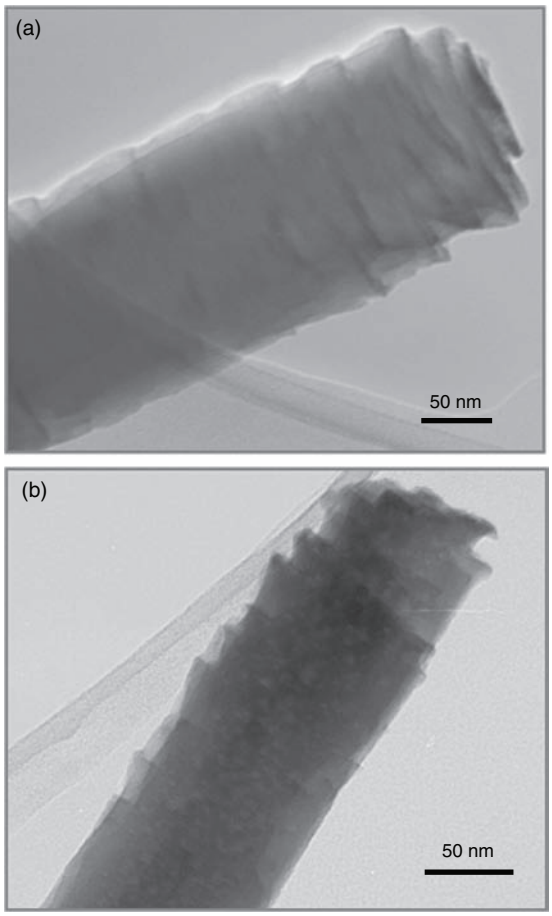


**Fig. 2.** Typical TEM images of ZnO:Sb nanorods of sample 3 (a) as-grown and (b) annealed at 500 °C in $O_2$ atmosphere.

Although a higher content of point defects in these nanorods that act as radiative centers can also account for their higher emission and cannot be discarded at this point.[25] CL images from antimony doped samples also show homogeneous CL intensity distribution as can be seen in Figures 3(c–h). EDS elemental mapping was performed on sample 3 in order to study the variation in chemical composition of the nanorods and nanoparticles. Figure 4(e) clearly shows that the nanoparticles have a higher Sb content than the nanorods, and as described before, the length of the rods decreases with increasing Sb concentration, until a particle-like morphology results from high Sb content (sample 4).

Figure 5(a) shows the room temperature CL spectra of the doped and undoped ZnO nanostructures. The CL spectrum of the undoped sample (curve 1) shows two well resolved emission bands centered around 3.14 and 2.09 eV, which are identified as the UV excitonic emission and the defect related yellow band, respectively. The CL spectra of the as-grown samples reveal that the incorporation of antimony in the ZnO nanostructures has a strong effect on their CL properties. Such effect is more evident in the heavily doped sample (sample 4), where the luminescence intensity decreased considerably, with no excitonic band detected, suggesting a strong lattice distortion and the presence of non-radiative defects. This quenching effect has been observed previously in ZnO:Sb layers, and attributed to the lattice distortion produced by incorporation of Sb atoms with a higher ionic radius (74 pm for $Zn^{2+}$, 90 pm for $Sb^{3+}$).[26] Figures 5(b) and (c) show the CL spectra acquired at room temperature of samples annealed in argon and oxygen atmospheres, respectively. They reveal an increase in the $I_{UV}/I_{yell}$ ratio for all samples, irrespective of the annealing atmosphere. It is worth noting that the thermal treatment of the samples in argon atmosphere substantially enhances the relative intensity of the excitonic emission, and therefore the magnitude of $I_{UV}/I_{yell}$ ratio.

CL spectra of all thermally treated samples (either in Ar or in $O_2$ atmosphere) show a red-shift of the yellow band. Such a red-shift might be due to the decrease in the relative emission intensity of a particular component of the broad yellow band. In a previous work we found that annealing ZnO nanorods in argon or oxygen atmosphere induces quenching of the emission band centered around 2.2 eV,

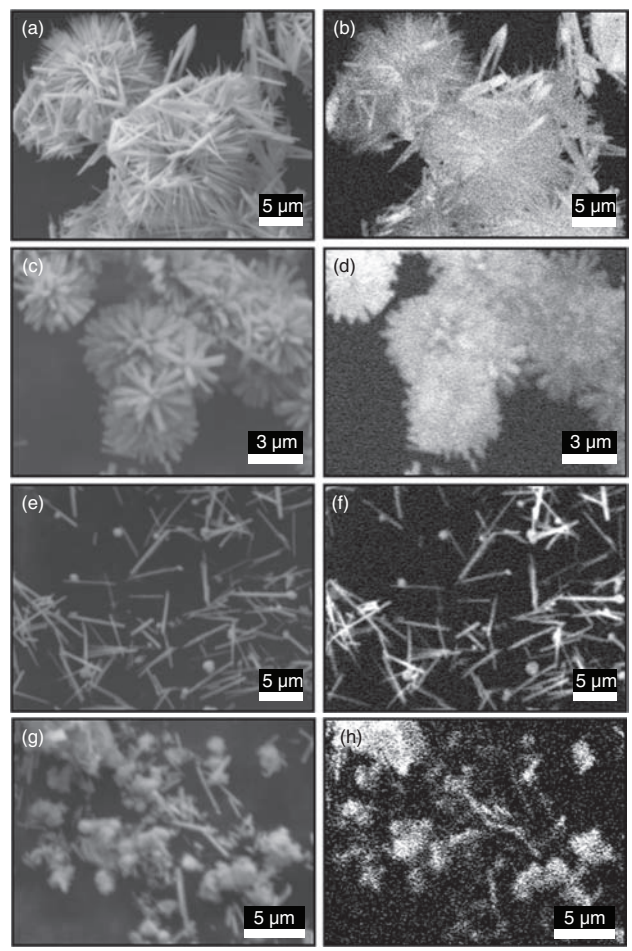


**Fig. 3.** Typical SEM images and their corresponding panchromatic CL images of ZnO:Sb nanorods. Sample 1 (a and b), sample 2 (c and d), sample 3 (e and f), and sample 4 (g and h).

RESEARCH ARTICLE

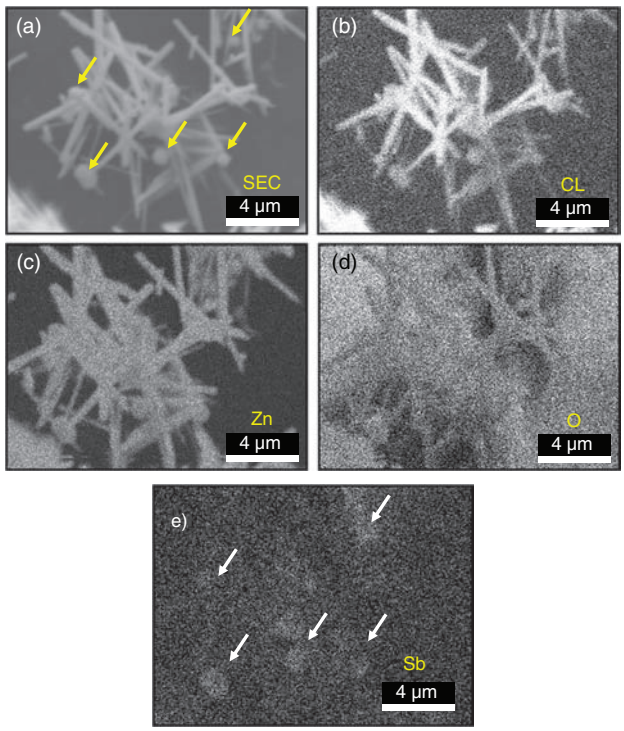


**Fig. 4.** Selected area (a) secondary, (b) CL images for the sample 3 and EDS elemental mapping for (c) zinc (K and L series), (d) oxygen (K series) and (e) antimony (L series) over the same area.



which has been identified as a sub-band of the broad yellow emission.[21] Although it was not possible to deconvolute the broad yellow band in the spectra of our sample to identify its components, we propose that thermal annealing decreases the intensity of this particular yellow sub-band located at about 2.2 eV causing the observed red-shift, an effect previously explained in terms of the annealing of interstitial Zn ($Zn_i$) defects in the ZnO lattice.[21]

Normalized low temperature (100 K) CL spectra of the as-grown samples [Fig. 6(a)] show a yellow band centered around 2.0 eV and an emerging shoulder in the blue region observed only in Sb doped samples, which increases in intensity as the Sb concentration is increased. Figure 6(b) shows the deconvoluted CL spectrum of the defect-related emissions for sample 3, revealing a blue emission band centered around of 2.74 eV. Formation of a similar blue band in Sb doped ZnO nanorods grown by the sol–gel method was reported by Ilican et al.[27] Such emission was associated with the formation of $Zn_i$ defects during synthesis. However, several authors have reported the presence of this blue emission in undoped ZnO.[28–29] Zheng et al. studied its origin in ZnO nanoshells using temperature-dependent photoluminescence, reporting that this emission in particular can be attributed to a strong localization effect of $Zn_i$ centers in ZnO.[30] The presence of the blue emission in our samples suggests that $Zn_i$ point defects could be formed by Sb doping.

Reported experimental work seems to support the proposed model of a complex $Sb_{Zn}$–$2V_{Zn}$ defect formation in *p*-type ZnO:Sb, with an activation energy between 100 and 200 meV above the valence band.[31–34] In order to generate a $Sb_{Zn}$–$2V_{Zn}$ defect, three Zn atoms are displaced from their lattice site thus forming $Zn_i$ defects. We believe that such mechanism is taking place in our annealed Sb doped nanostructures with the incorporation of Sb atoms in the ZnO lattice.

Comparing the CL spectra of the as-grown samples shown in Figures 5(a) and 6(a) it can be seen that temperature has a noticeable effect on the yellow emission band: at low temperature the band shifts to lower energies and becomes narrower, i.e., the full width at half maximum value (FWHM) decreases from 770 meV at room temperature to 570 meV at 100 K. It is worth to note that the relative intensity of blue emission in as-grown doped samples increases at lower temperatures [Fig. 6(a)]. Since the red-shift of the yellow band has been associated to annealing of $Zn_i$, and the generation of the blue emission is assigned to presence of $Zn_i$ defects, we propose that a competitive process between electronic transitions responsible for these emissions is taking place.

Finally, the low temperature CL spectra of annealed samples, either in Ar or $O_2$ atmospheres, revealed a

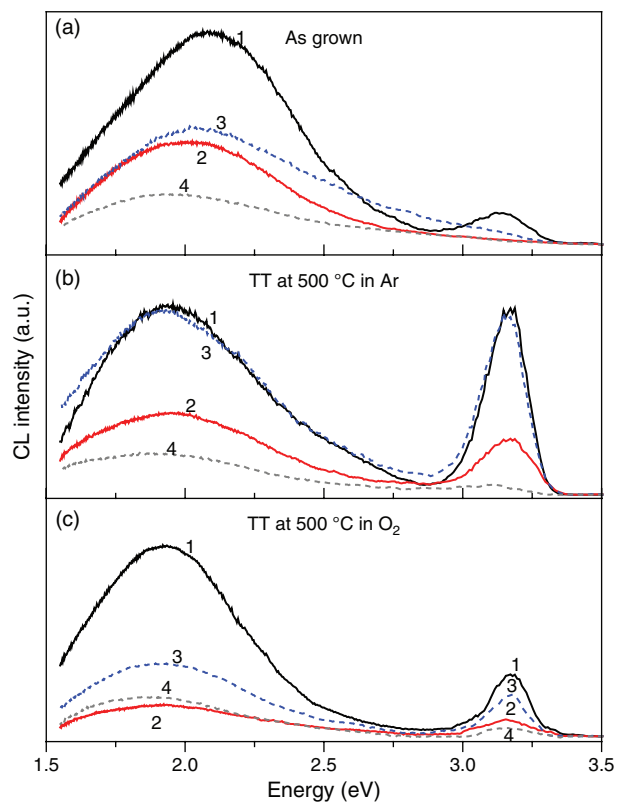


**Fig. 5.** Room temperature CL spectra of doped and undoped nanostructures: (a) As grown, (b) after thermal treatment at 500 °C in Ar, and (c) after thermal treatment at 500 °C in $O_2$ atmosphere. Spectra marked as 1,2,3 and 4 correspond to the samples 1,2,3, and 4, respectively.

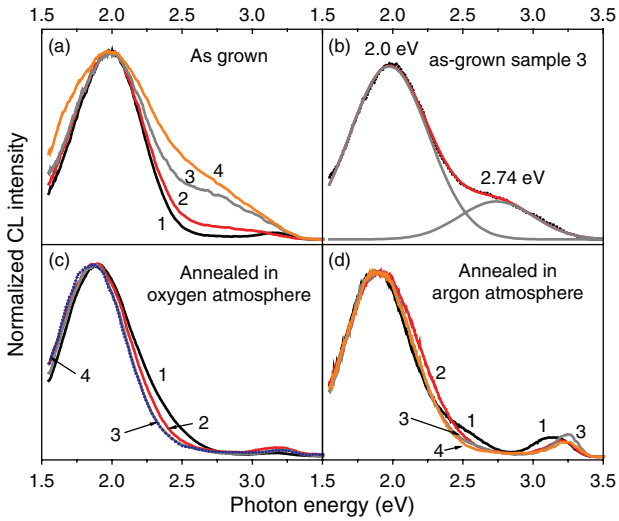


**Fig. 6.** Normalized CL spectra of doped and undoped nanostructures acquired at 100 K. Spectra marked as 1,2,3 and 4 correspond to the samples 1,2,3, and 4, respectively.

red-shift of the yellow band when compared their spectra before annealing, also an increase of the $I_{UV}/I_{yell}$ ratio, and quenching of the blue emission [Figs. 6(c and d)]. As mentioned above, the red-shift of the yellow band can be attributed to a decrease in the relative intensity of the yellow sub-band centered at 2.2 eV. The increase in the $I_{UV}/I_{yell}$ ratio is a result of the decrease of radiative defects, like $Zn_i$, which has been shown to be a common native defect with a high thermal diffusivity, which can be annealed at temperatures as low as 90–130 K,[35–37] same origin might be applied to the observed quenching of blue emission in doped samples.

## 4. CONCLUSIONS

Samples with different antimony contents were synthesized in order to study the effect of doping concentration on the morphology and optical properties of ZnO nanorods. Incorporation of Sb during growth resulted in the formation of nanorods with small aspect ratio, together with some Sb-rich nanoparticles. TEM measurements of the sample with 5 at% of Sb revealed delaminated {10–10} planes produced by antimony surface segregation. CL spectra of the as-grown samples revealed the presence of a blue band centered 2.74, with an intensity dependency on Sb content, indicating the formation of point defects due to Sb incorporation. We propose formation of $Zn_i$ during the antimony incorporation in ZnO nanorods, which easily disappeared upon annealing at 500 °C in Ar and $O_2$ atmospheres due to its high thermal diffusivity.

**Acknowledgments:** This work was supported by PAPIIT-UNAM (Grants No. IN107208 and IN107808). Technical help from E. Flores, E. Aparicio, F. Ruiz are acknowledged. The authors also would to thank N. Pineda (CIMAV-Monterrey) for her technical assistance in the ICP measurements.

## References and Notes

1. S. Nakamura, S. Pearton, and G. Fasol, The Blue Laser Diode, 2nd edn., Springer, Berlin **(2000)**.
2. S. A. Michael, Ph. Avouris, Z. W. Pan, and Z. L. Wang, *J. Phys. Chem. B* 107, 659 **(2003)**.
3. E. Comini, G. Faglia, G. Sberveglieri, Z. Pan, and Z. L. Wang, *Appl. Phys. Lett.* 81, 1869 **(2002)**.
4. K. Keis, L. Vayssieres, S. E. Lindquist, and A. Hagfeldt, *Nanostruct. Mater.* 12, 487 **(1999)**.
5. G. Srinivasan, R. T. Rajendra Kumar, and J. Kumar, *Opt. Mater.* 30, 314 **(2007)**.
6. D. Y. Ku, I. H. Kim, I. Lee, K. S. Lee, T. S. Lee, J. -H. Jeong, B. Cheong, Y. -J. Baik, and W. M. Kim, *Thin Solid Films* 515, 1364 **(2006)**.
7. Y. Caglar, S. Ilican, M. Caglar, and F. Yakuphanoglu, *Spectrochim. Acta Part A* 67, 1113 **(2007)**.
8. L. J. Mandalapu, F. X. Xiu, Z. Yang, and J. L. Liu, *Solid-State Electron.* 51, 1014 **(2007)**.
9. S. Ilican, Y. Caglar, M. Caglar, and F. Yakuphanoglu, *Physica E* 35, 131 **(2006)**.
10. A. Tsukazaki, A. Ohtomo, T. Onuma, M. Ohtani, T. Makino, M. Sumiya, K. Ohtani, S. F. Chichibu, S. Fuke, Y. Segawa, H. Ohno, H. Koinuma, and M. Kawasaki, *Nat. Mater.* 4, 42 **(2005)**.
11. J. G. Lu, Z. Z. Ye, F. Zhuge, Y. J. Zeng, B. H. Zhao, and L. P. Zhu, *Appl. Phys. Lett.* 85, 3134 **(2004)**.
12. D. K. Hwang, H. S. Kim, J. H. Lim, J. Y. Oh, J. H. Yang, S. J. Park, K. K. Kim, D. C. Look, and Y. S. Park, *Appl. Phys. Lett.* 86, 151917 **(2005)**.
13. F. X. Xiu, Z. Yang, L. J. Mandalapu, D. T. Zhao, and J. L. Liu, *Appl. Phys. Lett.* 87, 252102 **(2005)**.
14. X. H. Pan, W. Guo, Z. Z. Ye, B. Liu, Y. Che, H. P. He, and Q. Pan, *J. Appl. Phys.* 105, 113516 **(2009)**.
15. G. Hong, Z. Mingyu, J. Hong, W. Xuanzhang, and Z. Zhiguo, *J. Alloys Compd.* 464, 234 **(2008)**.
16. L. J. Mandalapu, Z. Yang, S. Chu, and J. L. Liu, *Appl. Phys. Lett.* 92, 122101 **(2008)**.
17. H. J. Fan, R. Scholz, M. Zacharias, U. Gösele, F. Bertam, D. Forster, and J. Christen, *Appl. Phys. Lett.* 85, 1601 **(2004)**.
18. D. Li, Y. H. Leung, A. B. Djurisic, Z. T. Liu, M. H. Xie, S. L. Shi, and S. J. Xu, *Appl. Phys. Lett.* 68, 403 **(1996)**.
19. K. Vanheusden, C. H. Seager, W. L. Warren, D. R. Tallant, and J. A. Voigt, *Appl. Phys. Lett.* 68, 403 **(1996)**.
20. A. F. Kohan, G. Ceder, D. Morgan, and C. G. Van de Walle, *Phys. Rev. B* 61, 15019 **(2000)**.
21. A. González, M. Herrera-Zaldívar, J. Valenzuela, A. Escobedo-Morales, and U. Pal. *Superlatices and Microstruct.* 45, 421 **(2009)**.
22. A. Escobedo-Morales, U. Pal, and M. Herrera-Zaldivar, *J. Nanosci. Nanotechnol.* 8, 6551 **(2008)**.
23. Z. Kai, Q. Xioa-Ying, D. Xiao-Feng, Z. Shao-Min, and Z. Xiao-Hong, *Appl. Phys. Lett.* 86, 013103 **(2005)**.
24. B. Aleman, P. Fernández, and J. Piqueras, *Appl. Phys. Lett.* 95, 013111 **(2009)**.
25. A. Urbieta, P. Fernández, and J. Piqueras, *Appl. Phys. Lett.* 85, 5968 **(2004)**.
26. O. Lopatiuk-Tirpak, W. V. Schoenfeld, L. Chernyak, F. X. Xiu, J. L. Liu, A. Osinsky, and P. Chow, *Appl. Phys. Lett.* 88, 202110 **(2006)**.
27. S. Ilican, Y. Caglar, M. Caglar, F. Yakuphanoglu, and J. Cui, *Physica E* 41, 96 **(2008)**.
28. W. Cheng, P. Wu, X. Zou, and T. Xiao, *J. Appl. Phys.* 100, 054311 **(2006)**.
29. Z. Y. Xue, D. H. Zhang, Q. P. Wang, and J. H. Wang, *Appl. Surf. Sci.* 195, 126 **(2002)**.

**30.** H. Zheng, Z. Li, W. Cai, and P. Liu, *J. Appl. Phys.* 102, 104307 **(2007)**.
**31.** X. Pan, Z. Ye, J. Li, X. Gu, Y. Zeng, H. He, L. Zhu, and Y. Che, *Appl. Surf. Sci.* 253, 5067 **(2007)**.
**32.** U. Wahl, J. G. Correia, T. Mondonça, and S. Decoster, *Appl. Phys. Lett.* 94, 261901 **(2009)**.
**33.** F. X. Xiu, Z. Yang, L. J. Mandalapu, D. T. Zhao, J. L. Liu, and W. P. Beyermann, *Appl. Phys. Lett*. 88, 152101 **(2005)**.
**34.** J. M. Qin, B. Yao, Y. Yan, J. Y. Zhang, X. P. Jia, Z. Z. Zhang, B. H. Li, C. X. Shan, and D. Z. Shen, *Appl. Phys Lett*. 95, 022101 **(2009)**.
**35.** A. Janotti and C. G. Van de Walle, *J. Cryst. Growth* 287, 58 **(2006)**.
**36.** D. G. Thomas, *J. Phys. Chem. Solids* 3, 299 **(1957)**.
**37.** P. Erhart and K. Albe, *Appl. Phys. Lett*. 88, 201918 **(2006)**.

Received: 11 November 2009. Revised/Accepted: 3 February 2010.